CMS Physics Analysis Summary

Contact: cms-pag-conveners-exotica@cern.ch 2021/05/24

Search for Higgs boson decays into long-lived particles in associated Z boson production

The CMS Collaboration

Abstract

We present a search for long-lived particles (LLPs) produced in association with a Z boson. The search is performed with data from 13 TeV proton-proton collisions recorded by the CMS experiment during 2016 − 2018, corresponding to an integrated luminosity of 117 fb^{-1}. The LLPs are assumed to decay into a pair of standard model fermions inside the tracker volume, which results in displaced jets. A trigger and selections based on Z boson decays to electron or muon pairs provide sensitivity to light (15 GeV or less) LLPs, which have up to now been difficult to access. Decays of LLPs are selected by requiring the presence of displaced jets which are identified using information from the CMS tracking system. The results are interpreted in the context of exotic decays of the Higgs boson to LLPs ($\text{H} \to \text{SS}$). The search is sensitive to branching fractions $\mathcal{B}(\text{H} \to \text{SS})$ of $4 - 5\%$ (less than 20%) for LLP masses of 40 (15) GeV and mean proper decay lengths of $10 - 100$ mm ($10 - 50$ mm).

1 Introduction

New long-lived particles (LLPs) with macroscopic decay lengths emerge from many extensions to the standard model (SM) of elementary particles. LLPs are found in a long list of models spanning supersymmetry [1–8], little Higgs [9], twin Higgs [10], hidden valleys [11, 12], and dark sectors [13–16]. LLPs may also play a role in explaining baryogenesis [17] or neutrino masses [18]. A general feature of these models is the production of LLPs in proton-proton (pp) collisions at the CERN Large Hadron Collider (LHC), which decay into SM particles far from the interaction point (IP).

A particularly interesting class of models are those proposing a form of neutral naturalness [19], where the hierarchy problem is solved by the existence of a top quark partner that is not color-charged under the SM $\mathrm{SU}(3)_c$ group but is instead charged under a mirror color group of a hidden sector, and thus evades the stringent experimental bounds on strongly produced particles. The Higgs boson (H) may decay into long-lived bound states of the mirror color group, which subsequently decay back into SM particles through kinetic mixing with the Higgs boson. This results in the production of LLPs in Higgs boson events at the LHC. The branching ratios of such LLPs are those of the off-shell Higgs boson, and are dominated by decays to a pair of quarks. LLP decays will therefore manifest themselves as displaced jets.

Existing LHC searches for displaced jets typically rely on a large jet transverse momentum in order to pass the trigger requirements, and thus have limited sensitivity for Higgs boson decays to displaced jets, where the resulting jets can have low transverse momentum (p_T). This note presents an alternative approach which exploits the unexplored associated production of the Higgs boson with a Z boson, where prompt leptons provide a performant trigger for events with low-p_T jets. Figure 1 shows a simplified model where the Higgs boson is produced in association with a Z boson, and subsequentely decays to a pair of long-lived scalars (S). In order to tag a jet as displaced we rely on information from the CMS tracking system, which results in the greatest sensitivity for mean proper decay lengths of around 10 cm. Searches for LLPs produced via the Higgs boson have been performed by the CMS [20] and ATLAS Collaborations [21–23], where the searches have focused on gluon fusion production of the Higgs boson.

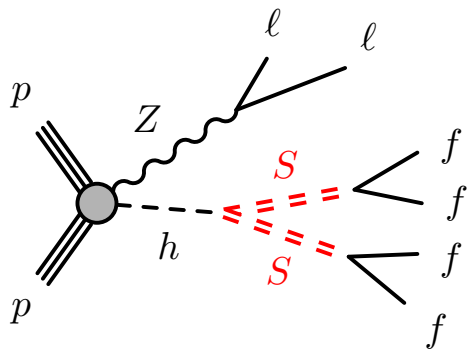

Figure 1: A simplified model for the Higgs boson decaying to a pair of long-lived scalars (S). The Higgs boson is produced in association with a Z boson, where the Z boson decays to pair of leptons. The long-lived scalars decay to a pair of fermions (f).

This note is organized as follows. A brief description of the CMS detector is given in Section 2. Section 3 describes the data and simulation samples used. Section 4 explains the displaced jet identification strategy and event selection. The background estimation technique is described in Section 5, and the treatment of systematic uncertainties is given in Section 6. Results for the

signal models described above are presented in Section 7.

2 The CMS detector

The central feature of the CMS apparatus is a superconducting solenoid of 6 m internal diameter, providing a magnetic field of 3.8 T. Within the solenoid volume are a silicon pixel and strip tracker, a lead tungstate crystal electromagnetic calorimeter (ECAL), and a brass and scintillator hadron calorimeter (HCAL), each composed of a barrel and two endcap sections. Forward calorimeters extend the pseudorapidity (η) coverage provided by the barrel and endcap detectors. Muons are measured in gas-ionization detectors embedded in the steel flux-return yoke outside the solenoid.

The silicon tracker measures charged particles within the pseudorapidity range $|\eta| < 2.5$ ($|\eta| < 3.0$) during the LHC running period in 2016 (2017–2018). For the data used in this note, the silicon tracker consisted of 1440 (1856) silicon pixel detector modules during the 2016 (2017–2018) running period and 15,148 silicon strip modules throughout the 2016–2018 run. For non-isolated particles of $1 < p_{\mathrm{T}} < 10\,\mathrm{GeV}$ and $|\eta| < 1.4$ ($|\eta| < 3.0$), the track resolutions are typically 1.5% in p_{T} and 25–90 μm (20–75 μm) in the transverse impact parameter, for the 2016 (2017–2018) running period [24].

In the region $|\eta| < 1.74$, the HCAL cells have widths of 0.087 in pseudorapidity and 0.087 in azimuth (ϕ). In the η-ϕ plane, and for $|\eta| < 1.48$, the HCAL cells map on to 5×5 arrays of ECAL crystals to form calorimeter towers projecting radially outwards from a point close to the nominal interaction point. For $|\eta| > 1.74$, the coverage of the towers increases progressively to a maximum of 0.174 in $\Delta\eta$ and $\Delta\phi$. Within each tower, the energy deposits in ECAL and HCAL cells are summed to define the calorimeter tower energies, which are subsequently used to provide the energies and directions of hadronic jets.

Events of interest are selected using a two-tiered trigger system [25]. The first level (L1), composed of custom hardware processors, uses information from the calorimeters and muon detectors to select events at a rate of around 100 kHz within a time interval of less than 4 μs. The second level, known as the high-level trigger (HLT), consists of a farm of processors running a version of the full event reconstruction software optimized for fast processing, and reduces the event rate to around 1 kHz before data storage. A more detailed description of the CMS detector, together with a definition of the coordinate system used and the relevant kinematic variables, can be found in Ref. [26].

3 Data and simulated samples

This search uses a sample of pp collisions at the LHC collected from 2016-2018 at $\sqrt{s} = 13\,\mathrm{TeV}$, corresponding to an integrated luminosity of $117\,\mathrm{fb}^{-1}$. During parts of the 2016 data-taking period there was an increased tracking inefficiency in certain regions of the tracker system which resulted in spurious displaced jets; therefore collision events which occurred during those times are excluded from this search.

Events in this search were recorded by use of lepton-based triggers. One set of triggers requires either two electrons or two muons with opposite charge, while another set of triggers requires different flavor dilepton pairs (i.e. eμ pairs).

The performance of the analysis on ZH events containing new LLPs is evaluated using simulated events. Quark- and gluon-initiated associated Higgs boson production are generated

with POWHEG 2.0 [27–32] with leading-order (LO) and next-to-LO (NLO) accuracy, respectively. Higgs boson decays to long-lived scalars are generated with PYTHIA 8.226 [33]. The scalar is simulated as a generic scalar particle with a 100% branching fraction to either b quarks or d quarks. The mass and lifetime of the scalar are varied according to the recommendations of the LHC Higgs cross section working group [34].

The Drell-Yan process, which is the main background in this search, is simulated at NLO in quantum chromodynamics (QCD) using the MADGRAPH5_aMC@NLO 2.4.2 [35] generator with up to two partons in the final state at the matrix element (ME) level. The corresponding cross section is calculated with FEWZ v3.1b2 [36] at next-to-NLO (NNLO) in QCD and NLO accuracy in electroweak (EW) theory. The $t\bar{t}$ background is simulated with NLO precision in QCD using the MADGRAPH5_aMC@NLO generator, and its cross section is obtained from the TOP++ v2.0 [37] prediction that includes NNLO corrections in QCD and resummation of the next-to-next-to-leading-logarithm (NNLL) soft gluon terms. The single-top quark processes are simulated at NLO in QCD via either POWHEG or MADGRAPH5_aMC@NLO and their cross sections are computed, at the same order of precision, using HATHOR [38]. For the simulated samples corresponding to the 2016 (2017–2018) data-taking periods, the NNPDF v3.0 (v3.1) NLO (NNLO) parton distribution functions (PDFs) are used [39, 40]. The CUETP8M1 tune [41] is used for the simulated samples corresponding to the 2016 data-taking period, while the CP5 tune [42] is used for the 2017 and 2018 simulated data. For processes generated at NLO (LO) in QCD with the MADGRAPH5_aMC@NLO generator, events from the ME characterized by different parton multiplicities are merged via the FxFx (MLM) prescription [43, 44]. The simulated events at the ME level for both the signal and background processes are interfaced with PYTHIA 8.2.2 or a later version [45] to simulate the shower and hadronization of partons in the initial and final states, along with the underlying event description.

For all simulated processes, the detector response is simulated using a detailed description of the CMS detector based on GEANT4 [46]. Object and event reconstruction are performed with the same algorithms as are used for the data. The simulated samples include the effect of multiple pp interactions per bunch crossing (pileup) and are weighted such that the pileup distribution matches the measured one during each data taking period.

4 Search strategy and selections

The basic strategy of this search is to use the number of displaced jets (N^{j}_{dis}) in the event to distinguish the signal from the backgrounds. Signal events typically contain $N^{j}_{dis} \geq 2$, while SM backgrounds exhibit a sharply falling distribution in N^{j}_{dis}.

Background events with displaced jets include known SM displaced decays, nuclear interactions with the tracker material, photon conversion, and mis-identification of prompt jets as displaced due to track-multiplicity and resolution effects. Since the simulation may not capture these effects perfectly, we use a data-driven strategy to estimate the number of misidentified jets from SM backgrounds, by looking at control samples of low-p_T opposite charge dilepton pairs (modeling the dominant SM Z production) and of different flavor lepton pairs (modeling the subdominant contribution from $t\bar{t}$ and single-top quark production). Rare backgrounds, including SM multiboson production, are estimated from simulation as their contribution to the signal sample is small.

The energy of each electron is determined from a combination of the electron momentum at the primary interaction vertex as determined by the tracker, the energy of the corresponding

ECAL cluster, and the energy sum of all bremsstrahlung photons spatially compatible with originating from the electron track [47]. The energy of each muon is obtained from the curvature of the corresponding track [48]. Electron pairs are required to have a minimum p_T of 25 (15) GeV for the leading (subleading) candidates, while for muon pairs the thresholds were 25 (12) GeV. Electron and muons are required to have $|\eta| < 2.5$ and $|\eta| < 2.4$, respectively. To further reduce fake leptons, additional requirements are applied to the reconstructed electron and muon candidates. The resulting efficiencies for electrons and for muons are above 90%.

Jets are reconstructed offline from the energy deposits in the calorimeter towers, clustered using the anti-k_T algorithm [49, 50] with a distance parameter of 0.4. In this process, the contribution from each calorimeter tower is assigned a momentum, the absolute value and the direction of which are given by the energy measured in the tower, and the coordinates of the tower. The raw jet energy is obtained from the sum of the tower energies, and the raw jet momentum by the vectorial sum of the tower momenta, which results in a nonzero jet mass. The raw jet energies are then corrected to establish a uniform relative response of the calorimeter in η, and a calibrated absolute response in transverse momentum p_T. Jets are required to have a minimum p_T of 35 GeV and to fall within the silicon strip tracker acceptance $|\eta| < 2.4$. Basic quality cuts are applied to suppress contributions from electronic noise, electrons and muons. Jets are subsequently used to select 'high-purity' tracks [24], with $p_T \geq 1$ GeV, which impact the calorimeter front-face near the jet direction. The selected tracks are used to evaluate whether or not the jet is displaced.

Having defined the objects used in the analysis, the search sample is defined as follows. Events are required to have a primary pp interaction vertex. Of the candidate vertices associated with a given proton-proton bunch crossing, the one with the largest value of summed physics-object p_T^2 is taken to be the primary pp interaction vertex. The physics objects are the jets, clustered using a jet finding algorithm [49, 50] with the tracks assigned to candidate vertices as inputs, and the associated missing transverse momentum, taken as the negative vector sum of the p_T of those jets. Additionally, there must be at least one opposite charge, same flavor lepton pair in the event. The lepton pair is required to have an invariant mass between 70 and 110 GeV and a p_T of at least 100 GeV. The p_T cut on the lepton pair serves to suppress Drell-Yan events with a typically low dilepton p_T, and enhance the contribution of associated Higgs boson production. We require zero additional leptons with p_T larger than 15 GeV, and at least one jet. In addition to the search sample, we define two control samples that are used for the background estimation presented in Section 5. The Z control sample has the same requirements as the signal sample, except the dilepton p_T must be at least 10 GeV and less than 100 GeV. A second control sample is used to estimate the background from $\mathrm{t\bar{t}}$ and single-top quark production, and is hereafter referred to as the top quark control sample. The top quark control sample is selected by requiring different flavor lepton pairs each with a p_T of at least 10 GeV.

The properties of the tracks associated with jets are used to calculate three displacement variables, as previously reported by the CMS Collaboration [51]. The three displacement variables, hereafter referred to as tagging variables, are used to identify displaced jets. The first tagging variable is the jet impact point significance ($\hat{\mathrm{IP}}^{\mathrm{2D}}_{\mathrm{sig}}$), where $\hat{\mathrm{IP}}^{\mathrm{2D}}_{\mathrm{sig}}$ is the median logarithm (base 10) of the individual track's impact point significance ($d_{xy}/\sigma_{d_{xy}}$), with d_{xy} being the track transverse impact parameter and $\sigma_{d_{xy}}$ its uncertainty. SM backgrounds, largely composed of prompt jets whose tracks display d_{xy} values of the order of $\sigma_{d_{xy}}$, exhibit an $\hat{\mathrm{IP}}^{\mathrm{2D}}_{\mathrm{sig}}$ value peaked near zero. On the other hand, displaced decays of LLPs tend to have jets with $\hat{\mathrm{IP}}^{\mathrm{2D}}_{\mathrm{sig}}$ values above 1.2, meaning

that the transverse impact parameter is highly significant (more than $15\sigma_{d_{xy}}$ from the interaction point). The second tagging variable is the jet transverse angle ($\hat{\Theta}^{2D}$), representing the angle between the jet-axis and the ray formed by connecting the primary vertex (PV) to the jet formation point; $\hat{\Theta}^{2D}$ is calculated as the median logarithm (base 10) of the angle between the track direction and the vector connecting its innermost hit in the silicon tracker to the PV. Prompt jets have angles near zero as the jet-axis is nearly the same as the ray which connects the PV to the jet formation point. In the case of LLPs, the directions of these vectors are not necessarily aligned, thus forming larger angles. The last tagging variable is α_{max}, which is calculated as follows: for each reconstructed vertex, we define α as the ratio of the summed-p_{T} for the tracks within the jet that are associated with that particular vertex to the total summed-p_{T} for all tracks within the jet. α_{max} corresponds to the maximum α value across all reconstructed vertices. LLPs forming displaced jets typically exhibit α_{max} values near zero, as the tracks belonging to these jets do not originate from any collision vertex.

Finally, we derive requirements for each of the three tagging variables obtained by finding the maximum discovery reach for this search. Jets are identified as displaced when $\hat{\text{IP}}^{2D}_{\text{sig}} > 1.25$, $\hat{\Theta}^{2D} > -1.5$, and $\alpha_{\text{max}} < 0.45$. The distribution of the number of displaced jets, $\text{N}^{\text{j}}_{\text{dis}}$, is then used to distinguish the signal from background; an excess of events where $\text{N}^{\text{j}}_{\text{dis}} \geq 2$ would indicate the presence of a signal.

5 Background estimation

The background estimation is carried out using the control samples defined in the previous section. Since the displaced jet tagging variables can be affected by a variety of instrumental effects, we use a data-driven technique to estimate the number of displaced jets in the search sample from the numbers in the control samples by performing a simultaneous binned maximum-likelihood fit. For each displaced jet multiplicity bin i, we define transfer factors from the control samples to the signal sample using simulation. Transfer factors are derived for the two main background sources: Z + jets and top quark (including $\text{t}\bar{\text{t}}$ and single-top) production. The Z + jets transfer factors (R^{Z}_{i}) are defined as the ratio of the yields in ith bin in the search sample to the corresponding bin in the Z control sample, where both yields are obtained from the Z + jets simulation. Similarly, the transfer factors for the top quark backgrounds (R^{t}_{i}) are the ratios of the yield in the ith bin in the search sample to the corresponding bin in the top quark control sample, where both yields are obtained from the simulation of $\text{t}\bar{\text{t}}$ and single-top quark processes. A third set of transfer factors ($R^{\text{t}\rightarrow\text{Z}}_{i}$) are used to account for the contamination from top quark backgrounds in the Z control sample. $R^{\text{t}\rightarrow\text{Z}}_{i}$ is defined as the ratio of the yields in the ith bin in the Z control sample to the corresponding bin in the top quark control sample, where both yields are obtained from the simulation of $\text{t}\bar{\text{t}}$ and single-top quark processes. The statistical uncertainty in the R_i values, due to the finite number of simulated events, is propagated to the final result.

The R_i values, their associated uncertainties, as well as the yields in the control and signal samples are used as the ingredients in a likelihood model which fits the background contributions and the signal yield. The fit is performed simultaneously across the signal and control samples. The background yields in the search sample, for each displaced jet multiplicity bin i, are the sum of the yields from the individual background processes. The contributions from the main background process (Z + jets and top quark production) in the signal sample are estimated as the product of the R_i values and a set of freely floating parameters which represent the yield in each of the i bins for a specific background process in the corresponding control

Table 1: Summary of the systematic uncertainties in the background and signal yield predictions. Dashes indicate that the systematic effect is not applicable for either the signal or the background, or is negligible.

Uncertainty source	Signal (%)	Background (%)
Luminosity	1.8	1.8
Dilepton trigger scale factors	1	1
Lepton energy scale	0.5–1	1–2
Lepton ID and ISO scale factors	1–2	—
Jet energy scale	4–8	2–4
Displaced-jet correction	1–20	1–5
Transfer factor (statistical)	—	1–90
Signal simulation sample size	1–10	—
Control region (statistical)	—	0.1–5

sample. By performing a fit in the signal and control samples we are able to simultaneously obtain: the per process yields in the control samples, the values of the transfer factors, and thus the estimated backgrounds in the signal sample.

The systematic uncertainties affecting the R_i transfer factors are included in the simultaneous fit. Each systematic uncertainty source is modeled as a log-normal constraint in the likelihood using a set of derived relative uncertainties (σ^i_{rel}) and a single normally distributed nuisance parameter x according to the expression $R_i(1+\sigma^i_{\text{rel}})^x$, such that the mean of the transfer factor is the central value extracted from the simulation. The statistical uncertainty on R_i due to the finite number of simulated events is propagated for each bin and is treated as uncorrelated among the bins.

For rare backgrounds such as SM multiboson events or Higgs boson decays, the contributions to the search sample are taken directly from the simulation, and correspond to less than 2% of the total background yield.

6 Systematic uncertainties

The main systematic uncertainties in the search are related to the possibility that the transfer factors obtained from the simulation do not accurately reflect the data. The main systematic sources are detailed in Table 1. In order to check the validity of the treatment of systematic uncertainties and rule out other possible systematic effects, we construct seven independent validation samples, by inverting the requirement on one or more of the displaced jet tagging variables, where the signal contamination in each validation sample is negligible. We perform the background estimation procedure for each validation region in the same fashion as in the main search sample, as detailed in Sec. 5. If the background estimation is working as intended and the treatment of the systematic uncertainties is adequate, we should find that the binned-likelihood model will accurately reproduce the displaced jet multiplicity distribution in all the validation samples.

No significant deviations are observed when performing the fit in the validation samples, thus validating the background estimation method and the treatment of systematics.

Table 1 summarizes the systematic uncertainties. The signal yield observed is directly affected by the uncertainty on the luminosity collected, estimated as 1.8% by a dedicated analysis [52–54]. Lepton energy scale uncertainties affect the efficiency of the Z mass constraint in the search sample; these are varied according to values extracted from a study of leptonic Z decays and

result in 1–2% uncertainties on both the signal and background yields. Lepton efficiency uncertainties are extracted from a tag-and-probe analysis and are also 1–2%. The pileup uncertainty is found to be negligible. Uncertainties in the jet energy scale affect the jet p_T selection efficiency at the level of 5–15%, and varying the shape of the displaced jet tagging variable distributions in the simulation to cover possible mismodeling of the data results in an uncertainty of between 1 and 20%, depending on the multiplicity bin. The statistical uncertainty in the transfer factors increases with the displaced jet multiplicity and reaches a maximum of 90% in the $N^j_{dis} \geq 2$ bin, thus representing the largest source of uncertainty in the search. The statistical uncertainty contribution in the signal sample from the control samples is found to be 0.1–5%. The statistical uncertainty on the backgrounds taken from the simulation is propagated and found to be negligible. The signal simulation statistical uncertainty is found to be 1–10% in the signal sample depending on the signal model and the N^j_{dis} bin.

7 Results and summary

The result of the background estimation procedure is compared with the observed data in Figure 2, where we show the content of the $N^j_{dis} \geq 2$ bin in each of the seven validation samples, along with the content in the signal sample. No excess in the data with respect to the SM background is observed. In the most sensitive bin in the signal sample, $N^j_{dis} \geq 2$, we observe 3 events with an expected background of 3.5 ± 1.8.

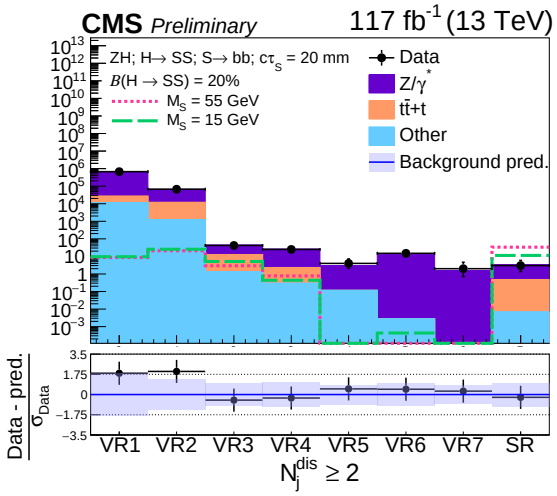

Figure 2: The background estimate and the observed data in the $N^j_{dis} \geq 2$ bins, for each of the seven validation samples along with the signal sample. Two signal model distributions for scalar masses of 15 and 55 GeV are also shown, where the Higgs boson branching ratio to long-lived scalars ($\mathcal{B}(H \to SS)$) is set to 20%.

We set upper limits on the Higgs boson branching ratio to a pair of long-lived scalars for different masses and as a function of the mean proper decay length of the scalar. We follow the LHC CL_s criterion [55, 56] by using the profile likelihood ratio test statistic and the asymptotic formula [57] to evaluate the 95% confidence level (CL) observed and expected limits on the Higgs boson branching ratio to a pair of long-lived scalars. Systematic uncertainties are propagated by incorporating nuisance parameters that represent different sources of systematic uncertainty, which are profiled in the maximum likelihood fit [58]. Two scenarios are considered, S decays to either a pair of b quarks or d quarks. The 95% CL upper limits are shown in Figure 3. We constrain the Higgs boson branching fraction to long-lived scalars decaying to

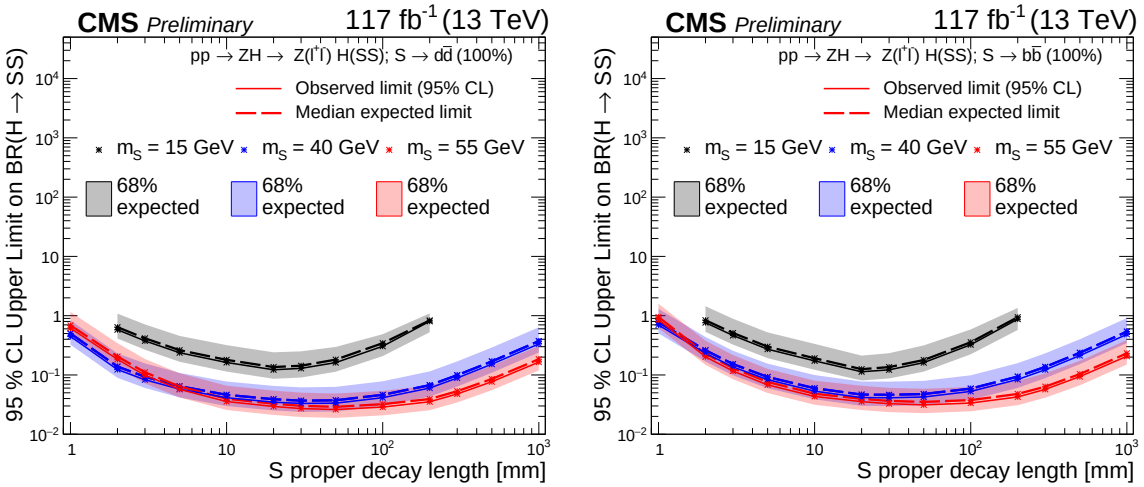

Figure 3: 95% CL exclusion limits on the Higgs boson branching ratio to long-lived scalars ($\mathcal{B}(\mathrm{H} \to \mathrm{SS})$). Limits are presented for scalar decays to d quarks (left) and b quarks (right) as a function of the mean proper decay length of the scalar. Different scalar masses are shown in different colors for each scalar decay mode.

d (b) quarks at the 3–4% (4–5%) level for masses of 40 GeV and 55 GeV and mean proper decay lengths in the 10–100 mm range. The upper bound on the Higgs branching ratio to 15 GeV long-lived scalars decaying to d quarks (b quarks) is about 14% (13%) in the 10–50 mm range of proper decay lengths. These exclusions are among the most stringent constraints on Higgs decaying to light (15 GeV or less) long-lived scalars which subsequently decay to a pair of b quarks.

8 Summary

We have performed a search for long-lived particles that are produced via Higgs boson decays to a pair of scalars in association with a Z boson, resulting in displaced jets. The Higgs boson decay branching ratio is constrained to be below 5–10% for proper decays lengths of 10–100 mm and masses between 40 and 55 GeV. This result yields stringent exclusion limits on exotic Higgs decays to long-lived scalars. In particular, this analysis provides the most stringent CMS limits for the branching fractions $\mathcal{B}(\mathrm{H} \to \mathrm{SS})$ for low mass scalar particles of around 15 GeV with mean proper decay lengths of 2–30 mm, where the scalars decay to a pair of b quarks.

References

[1] A. Arvanitaki, N. Craig, S. Dimopoulos, and G. Villadoro, "Mini-split", *JHEP* **02** (2013) 126, doi:10.1007/JHEP02(2013)126, arXiv:1210.0555.

[2] N. Arkani-Hamed et al., "Simply unnatural supersymmetry", 2012. arXiv:1212.6971.

[3] G. F. Giudice and R. Rattazzi, "Theories with gauge mediated supersymmetry breaking", *Phys. Rept.* **322** (1999) 419, doi:10.1016/S0370-1573(99)00042-3, arXiv:hep-ph/9801271.

[4] R. Barbier et al., "*R*-parity violating supersymmetry", *Phys. Rept.* **420** (2005) 1, doi:10.1016/j.physrep.2005.08.006, arXiv:hep-ph/0406039.

[5] C. Csaki, E. Kuflik, and T. Volansky, "Dynamical R-parity Violation", *Phys. Rev. Lett.* **112** (2014) 131801, doi:10.1103/PhysRevLett.112.131801, arXiv:1309.5957.

[6] J. Fan, M. Reece, and J. T. Ruderman, "Stealth supersymmetry", *JHEP* **11** (2011) 012, doi:10.1007/JHEP11(2011)012, arXiv:1105.5135.

[7] J. Fan, M. Reece, and J. T. Ruderman, "A stealth supersymmetry sampler", *JHEP* **07** (2012) 196, doi:10.1007/JHEP07(2012)196, arXiv:1201.4875.

[8] G. Burdman, Z. Chacko, H.-S. Goh, and R. Harnik, "Folded supersymmetry and the LEP paradox", *JHEP* **02** (2007) 009, doi:10.1088/1126-6708/2007/02/009, arXiv:hep-ph/0609152.

[9] H. Cai, H.-C. Cheng, and J. Terning, "A quirky little Higgs model", *JHEP* **05** (2009) 045, doi:10.1088/1126-6708/2009/05/045, arXiv:0812.0843.

[10] Z. Chacko, H.-S. Goh, and R. Harnik, "The Twin Higgs: Natural electroweak breaking from mirror symmetry", *Phys. Rev. Lett.* **96** (2006) 231802, doi:10.1103/PhysRevLett.96.231802, arXiv:hep-ph/0506256.

[11] M. J. Strassler and K. M. Zurek, "Echoes of a hidden valley at hadron colliders", *Phys. Lett. B* **651** (2007) 374, doi:10.1016/j.physletb.2007.06.055, arXiv:hep-ph/0604261.

[12] M. J. Strassler and K. M. Zurek, "Discovering the Higgs through highly-displaced vertices", *Phys. Lett. B* **661** (2008) 263, doi:10.1016/j.physletb.2008.02.008, arXiv:hep-ph/0605193.

[13] M. Baumgart et al., "Non-Abelian dark sectors and their collider signatures", *JHEP* **04** (2009) 014, doi:10.1088/1126-6708/2009/04/014, arXiv:0901.0283.

[14] D. E. Kaplan, M. A. Luty, and K. M. Zurek, "Asymmetric dark matter", *Phys. Rev. D* **79** (2009) 115016, doi:10.1103/PhysRevD.79.115016, arXiv:0901.4117.

[15] K. R. Dienes and B. Thomas, "Dynamical dark matter: I. Theoretical overview", *Phys. Rev. D* **85** (2012) 083523, doi:10.1103/PhysRevD.85.083523, arXiv:1106.4546.

[16] K. R. Dienes, S. Su, and B. Thomas, "Distinguishing dynamical dark matter at the LHC", *Phys. Rev. D* **86** (2012) 054008, doi:10.1103/PhysRevD.86.054008, arXiv:1204.4183.

[17] Y. Cui and B. Shuve, "Probing baryogenesis with displaced vertices at the LHC", *JHEP* **02** (2015) 049, doi:10.1007/JHEP02(2015)049, arXiv:1409.6729.

[18] B. Batell, M. Pospelov, and B. Shuve, "Shedding Light on Neutrino Masses with Dark Forces", *JHEP* **08** (2016) 052, doi:10.1007/JHEP08(2016)052, arXiv:1604.06099.

[19] Z. Chacko, D. Curtin, and C. B. Verhaaren, "A quirky probe of neutral naturalness", *Phys. Rev. D* **94** (2016) 011504, doi:10.1103/PhysRevD.94.011504, arXiv:1512.05782.

[20] CMS Collaboration, "Search for long-lived particles using displaced jets in proton-proton collisions at $\sqrt{s} = 13$ TeV", 12, 2020. arXiv:2012.01581. Submitted to *Phys. Rev. D*.

[21] ATLAS Collaboration, "Search for long-lived particles produced in pp collisions at $\sqrt{s} = 13$ TeV that decay into displaced hadronic jets in the ATLAS muon spectrometer", *Phys. Rev. D* **99** (2019) 052005, doi:10.1103/PhysRevD.99.052005, arXiv:1811.07370.

[22] ATLAS Collaboration, "Search for long-lived neutral particles in pp collisions at $\sqrt{s} = 13$ TeV that decay into displaced hadronic jets in the ATLAS calorimeter", *Eur. Phys. J. C* **79** (2019) 481, doi:10.1140/epjc/s10052-019-6962-6, arXiv:1902.03094.

[23] ATLAS Collaboration, "Search for long-lived neutral particles produced in pp collisions at $\sqrt{s} = 13$ TeV decaying into displaced hadronic jets in the ATLAS inner detector and muon spectrometer", *Phys. Rev. D* **101** (2020) 052013, doi:10.1103/PhysRevD.101.052013, arXiv:1911.12575.

[24] CMS Collaboration, "Description and performance of track and primary-vertex reconstruction with the CMS tracker", *JINST* **9** (2014) P10009, doi:10.1088/1748-0221/9/10/P10009, arXiv:1405.6569.

[25] CMS Collaboration, "The CMS trigger system", *JINST* **12** (2017) P01020, doi:10.1088/1748-0221/12/01/P01020, arXiv:1609.02366.

[26] CMS Collaboration, "The CMS experiment at the CERN LHC", *JINST* **3** (2008) S08004, doi:10.1088/1748-0221/3/08/S08004.

[27] P. Nason, "A New method for combining NLO QCD with shower Monte Carlo algorithms", *JHEP* **11** (2004) 040, doi:10.1088/1126-6708/2004/11/040, arXiv:hep-ph/0409146.

[28] S. Frixione, P. Nason, and C. Oleari, "Matching NLO QCD computations with Parton Shower simulations: the POWHEG method", *JHEP* **11** (2007) 070, doi:10.1088/1126-6708/2007/11/070, arXiv:0709.2092.

[29] S. Alioli, P. Nason, C. Oleari, and E. Re, "A general framework for implementing NLO calculations in shower Monte Carlo programs: the POWHEG BOX", *JHEP* **06** (2010) 043, doi:10.1007/JHEP06(2010)043, arXiv:1002.2581.

[30] S. Alioli, P. Nason, C. Oleari, and E. Re, "NLO single-top production matched with shower in POWHEG: s- and t-channel contributions", *JHEP* **09** (2009) 111, doi:10.1088/1126-6708/2009/09/111, arXiv:0907.4076. [Erratum: JHEP 02, 011 (2010)].

[31] E. Re, "Single-top Wt-channel production matched with parton showers using the POWHEG method", *Eur. Phys. J. C* **71** (2011) 1547, doi:10.1140/epjc/s10052-011-1547-z, arXiv:1009.2450.

[32] G. Luisoni, P. Nason, C. Oleari, and F. Tramontano, "$HW^{\pm}$/HZ + 0 and 1 jet at NLO with the POWHEG BOX interfaced to GoSam and their merging within MiNLO", *JHEP* **10** (2013) 083, doi:10.1007/JHEP10(2013)083, arXiv:1306.2542.

[33] T. Sjostrand, S. Mrenna, and P. Z. Skands, "PYTHIA 6.4 physics and manual", *JHEP* **05** (2006) 026, doi:10.1088/1126-6708/2006/05/026, arXiv:hep-ph/0603175.

[34] LHC Higgs Cross Section Working Group Collaboration, "Handbook of LHC Higgs Cross Sections: 4. Deciphering the Nature of the Higgs Sector", doi:10.23731/CYRM-2017-002, arXiv:1610.07922.

[35] J. Alwall et al., "The automated computation of tree-level and next-to-leading order differential cross sections, and their matching to parton shower simulations", *JHEP* **07** (2014) 079, doi:10.1007/JHEP07(2014)079, arXiv:1405.0301.

[36] Y. Li and F. Petriello, "Combining QCD and electroweak corrections to dilepton production in FEWZ", *Phys. Rev. D* **86** (2012) 094034, doi:10.1103/PhysRevD.86.094034, arXiv:1208.5967.

[37] M. Czakon and A. Mitov, "Top++: A Program for the Calculation of the Top-Pair Cross-Section at Hadron Colliders", *Comput. Phys. Commun.* **185** (2014) 2930, doi:10.1016/j.cpc.2014.06.021, arXiv:1112.5675.

[38] P. Kant et al., "HatHor for single top-quark production: Updated predictions and uncertainty estimates for single top-quark production in hadronic collisions", *Comput. Phys. Commun.* **191** (2015) 74, doi:10.1016/j.cpc.2015.02.001, arXiv:1406.4403.

[39] NNPDF Collaboration, "Parton distributions for the LHC Run II", *JHEP* **04** (2015) 040, doi:10.1007/JHEP04(2015)040, arXiv:1410.8849.

[40] NNPDF Collaboration, "Parton distributions from high-precision collider data", *Eur. Phys. J. C* **77** (2017) 663, doi:10.1140/epjc/s10052-017-5199-5, arXiv:1706.00428.

[41] CMS Collaboration, "Event generator tunes obtained from underlying event and multiparton scattering measurements", *Eur. Phys. J. C* **76** (2016), no. 3, 155, doi:10.1140/epjc/s10052-016-3988-x, arXiv:1512.00815.

[42] CMS Collaboration, "Extraction and validation of a new set of CMS PYTHIA 8 tunes from underlying-event measurements", *Eur. Phys. J. C* **80** (2020) 4, doi:10.1140/epjc/s10052-019-7499-4, arXiv:1903.12179.

[43] J. Alwall et al., "Comparative study of various algorithms for the merging of parton showers and matrix elements in hadronic collisions", *Eur. Phys. J. C* **53** (2008) 473, doi:10.1140/epjc/s10052-007-0490-5, arXiv:0706.2569.

[44] R. Frederix and S. Frixione, "Merging meets matching in MC@NLO", *JHEP* **12** (2012) 061, doi:10.1007/JHEP12(2012)061, arXiv:1209.6215.

[45] T. Sjöstrand et al., "An introduction to PYTHIA 8.2", *Comput. Phys. Commun.* **191** (2015) 159, doi:10.1016/j.cpc.2015.01.024, arXiv:1410.3012.

[46] GEANT4 Collaboration, "GEANT 4: A Simulation toolkit", *Nucl. Instrum. Meth. A* **506** (2003) 250, doi:10.1016/S0168-9002(03)01368-8.

[47] CMS Collaboration, "Performance of electron reconstruction and selection with the CMS detector in proton-proton collisions at $\sqrt{s} = 8\,\text{TeV}$", *JINST* **10** (2015) P06005, doi:10.1088/1748-0221/10/06/P06005, arXiv:1502.02701.

[48] CMS Collaboration, "Performance of the CMS muon detector and muon reconstruction with proton-proton collisions at $\sqrt{s} = 13\,\text{TeV}$", *JINST* **13** (2018) P06015, doi:10.1088/1748-0221/13/06/P06015, arXiv:1804.04528.

[49] M. Cacciari, G. P. Salam, and G. Soyez, "The anti-k_t jet clustering algorithm", *JHEP* **04** (2008) 063, doi:10.1088/1126-6708/2008/04/063, arXiv:0802.1189.

[50] M. Cacciari, G. P. Salam, and G. Soyez, "FastJet user manual", *Eur. Phys. J. C* **72** (2012) 1896, doi:10.1140/epjc/s10052-012-1896-2, arXiv:1111.6097.

[51] CMS Collaboration, "Search for new long-lived particles at $\sqrt{s} = 13$ TeV", *Phys. Lett. B* **780** (2018) 432, doi:10.1016/j.physletb.2018.03.019, arXiv:1711.09120.

[52] CMS Collaboration, "CMS luminosity measurements for the 2016 data taking period", Technical Report CMS-PAS-LUM-17-001, 2017.

[53] CMS Collaboration, "CMS luminosity measurement for the 2017 data-taking period at $\sqrt{s} = 13$ TeV", Technical Report CMS-PAS-LUM-17-004, 2018.

[54] CMS Collaboration, "Cms luminosity measurement for the 2018 data-taking period at $\sqrt{s} = 13$ TeV", Technical Report CMS-PAS-LUM-18-002, 2019.

[55] A. L. Read, "Presentation of search results: The CL_s technique", *J. Phys. G* **28** (2002) 2693, doi:10.1088/0954-3899/28/10/313.

[56] T. Junk, "Confidence level computation for combining searches with small statistics", *Nucl. Instrum. Meth. A* **434** (1999) 435, doi:10.1016/S0168-9002(99)00498-2, arXiv:hep-ex/9902006.

[57] G. Cowan, K. Cranmer, E. Gross, and O. Vitells, "Asymptotic formulae for likelihood-based tests of new physics", *Eur. Phys. J. C* **71** (2011) 1554, doi:10.1140/epjc/s10052-011-1554-0, arXiv:1007.1727. [Erratum: doi:10.1140/epjc/s10052-013-2501-z].

[58] The ATLAS Collaboration, The CMS Collaboration, The LHC Higgs Combination Group, "Procedure for the LHC Higgs boson search combination in Summer 2011", Technical Report CMS-NOTE-2011-005, ATL-PHYS-PUB-2011-11, 2011.